PAPER

Microgels or microcapsules? Role of morphology on the release kinetics of thermoresponsive PNIPAm-*co*-PEGMa hydrogels†

Tatiya Trongsatitkul and Bridgette M. Budhlall*

The effect of morphology of PNIPAm, PEGMa and PNIPAm-*co*-PEGMa hydrogels on the uptake and delivery (release kinetics) of a model drug (FITC–dextran) was investigated. Two types of hydrogel architectures: microgels and microcapsules, without and with core–shell morphology, were synthesized. The microcapsules had 30–50% greater uptake compared to the corresponding microgel architecture. The estimated pore size for the PNIPAm, PNIPAm-*co*-PEGMa and PEGMa hydrogels were 78, 92 and 130 Å, respectively. The drug release was performed at 25, 37 (physiological temperature), and 45 °C (targeted stimulating temperature). Diffusion coefficients at temperatures below VPTT of the microgels showed close correlation with the pore size, but this was not the case for the microcapsules. The release kinetics is dominated by temperature responsiveness at T greater than the VPTT and by hydrogel morphology at $T <$ VPPT. There is a striking advantage of using temperature responsive PNIPAm on the release kinetics. In fact, in both PNIPAm and its copolymer with PEG, a quick burst release is observed at $T >$ VPTT. More than 80% of the drug was released in the first 10 min using the temperature responsive microcapsule, compared to 1 h for the corresponding microgel. Unlike prior reports in the literature, the release of FITC–dextran is characteristic of a Super Case II Fickian diffusion and Anomalous release mechanism for the copolymer microgels when $T >$ VPTT and for the PNIPAm and PEGMa microgels when $T <$ VPTT. These results demonstrate the feasibility of modulating the release profile of encapsulated proteins (for tissue repair), chemotherapeutics (for drug delivery) and nucleic acids (for gene delivery) by tailoring the polymer morphology.

1 Introduction

Poly(*N*-isopropylacrylamide) (PNIPAm) hydrogel has been widely studied for various potential applications.[1–3] Biomedical applications such as tissue engineering[4–6] and controlled drug delivery[7–14] are among the most intensively and extensively studied. This is due to PNIPAm possessing a sharp lower critical solution temperature (LCST) at 32 °C.[15–17]

A hydrated hydrogel of crosslinked PNIPAm collapses at the volume phase transition temperature (VPTT) corresponding to its polymer's LCST.[18,19] The collapsed PNIPAm hydrogel expels its liquid content and provides a mechanism for controlled-release. For controlled-release applications, VPTT can be tailored to human body temperature (37 °C). Increasing the VPTT can be achieved by hydrophilically modifying PNIPAm with copolymers such as poly(ethylene glycol) (PEG)[20–25] or acrylamide (Am).[26–28] Copolymerizing PNIPAm with PEG offers

Department of Plastics Engineering and NSF Center for High-Rate Nanomanufacturing, University of Massachusetts, Lowell, MA, 01854, USA. E-mail: Bridgette_Budhlall@uml.edu

† Electronic supplementary information (ESI) available. See DOI: 10.1039/c2py20889j

additional benefits for biomedical applications. It increases the response temperature to a biologically useful temperature and also improves biocompatibility.[20,24,29]

Thermally induced release is useful in applications where subtle changes in temperature can occur. Temperature changes in hydrogels can result in a phase change transition, transforming a swollen, hydrated state to a shrunken, dehydrated state. Also, PNIPAm microcapsules can burst from increased internal pressure (osmotic) upon contraction of the capsule shell wall due to the increase in temperature.

It is widely accepted that the release behavior from hydrogels is a complex process.[2] Parameters that have been shown to play important role in delivery properties, include drug–polymer network affinity, crosslink density, and relative drug molecular weight to pore size, architecture, glass transition temperature and molecular relaxation of the hydrogels as well as on the drug loading method.[30] The mechanism of both uptake and release is mainly governed by diffusion and/or swelling/shrinkage.[31] For this reason the models most applied are still based on Fick's second law of diffusion.[32] Furthermore, the morphology or structure of a hydrogel also plays an important role in release kinetics. An understanding of the role of polymer architecture is

therefore critical to engineering biomedical devices with the desired controlled-release functionality.

There are two major types of diffusion-controlled systems classified by the hydrogel structure; (1) matrix devices and (2) reservoir devices. Drug release from each type of system occurs by diffusion through the polymer mesh or through the water-filled pores. Matrix devices have simple geometries and the drug is dispersed throughout the three-dimensional structure of the hydrogel. It is impossible to obtain time independent or zero-order release in this type of system. On the other hand, with the reservoir devices (with more complex geometries *e.g.* core–shell), the rate-limiting step for drug release is diffusion through the outer membrane of the device.

In our previous study, we reported on the synthesis and characterization of multicore microcapsules of PNIPAm-based hydrogels.[24] Multiple-core morphology obtained *via* a double emulsion process was characterized by optical and laser scanning confocal microscopy (LSCM) and theoretically confirmed by spreading coefficient calculations. This multicore–shell morphology of the microcapsule may be classified as a reservoir system. With multiple cores however, a more complicated release mechanism is expected. The multicore feature may alter the osmotic pressure between the cores which controls the release mechanism in these systems.

Of equal importance in selecting either a microgel or microcapsule as a drug delivery device is the ability to incorporate specific materials within the hydrogel *i.e.* whether the cargo is aqueous, organic or inorganic.

In the present study, the matrix device (microgels) was compared to the reservoir device (multicore–shell microcapsules), composed of a copolymer of PNIPAm, acrylamide (Am), and polyethylene glycol monomethyl ether monomethacrylate (PEGMa) crosslinked with *N,N'*-methylenebisacrylamide (MBAm), in order to investigate the role of morphology on the thermally induced release of a model drug, FITC–dextran. The effect of the polymer hydrogel morphologies on the release kinetics was investigated at physiologically important temperatures (25, 37, and 45 °C) and environments (*i.e.* at pH 7.4). The types of diffusion mechanisms were also identified using the power law equation proposed by Peppas and Ritger[33] In this article, we also discuss the relative role of polymer type, drug and polymer network affinity, and relative drug molecular weight to pore size.

2 Experimental section

2.1 Materials

All chemicals used in this study were purchased from Sigma-Aldrich (Milwaukee, WI) unless otherwise noted, and were used as-received without further purification. *N*-Isopropylacrylamide (NIPAm), and acrylamide (Am) were used as comonomers. *N,N'*-Methylenebisacrylamide (MBAm) was used as crosslinker. Polyethylene glycol monomethyl ether monomethacrylate (PEGMa) macromonomer with M_n of 300 g mol^{-1} was used as comonomer. Silicone oil (DC710) was used as the core-oil. Light mineral oil was used as the continuous phase.
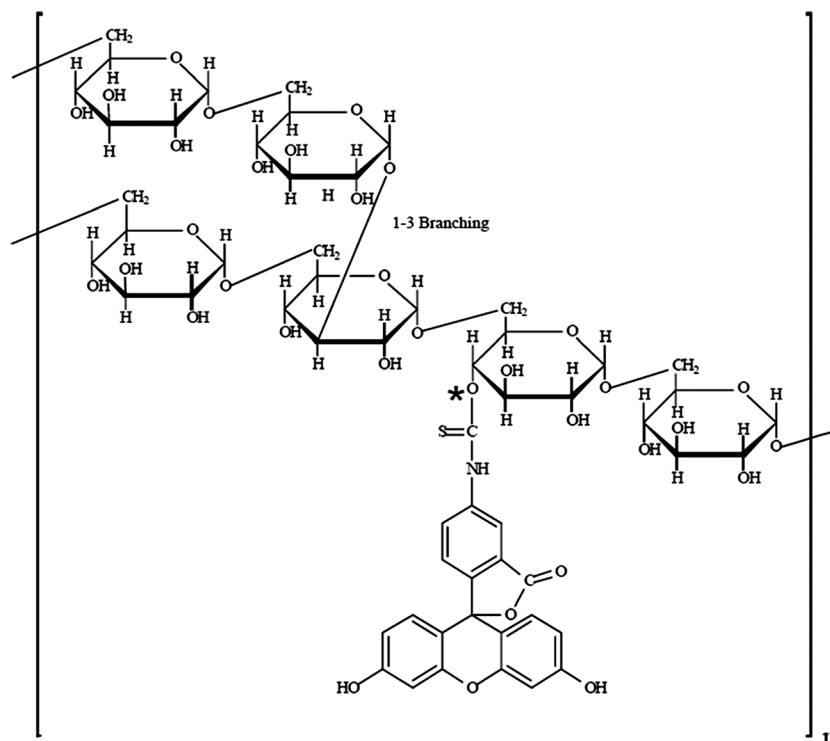
Scheme 1 Structural representation of a fragment of FITC–dextran molecule (from http://www.sigmaaldrich.com). The molecular weight of FITC–dextran used in the present study is 70 kDa with a hydrodynamic Stokes radius of 58 Å.[34]

2,2-Dimethoxy-2-phenylacetophenone and anthraquinone-2-sulfonic acid sodium salt monohydrate were used as an oil-soluble and water-soluble photoinitiators, respectively. Fluorescein isocyanate (FITC) labeled dextran (M_w 70 kDa) was chosen as a water-soluble model drug (Scheme 1). Deionized (DI) water was purified using the Millipore Elix 3 system (18 MΩ cm) and was used in all experiments.

A microarray technique was used to synthesize the thermoresponsive microgels and microcapsules. This technique allowed for real-time observations under a microscope and only requires a small amount of materials. A detailed description of this technique together with a summary of the chemical compositions of PNIPAm-based hydrogel has been described elsewhere.[24] Briefly, PDMS (Sylgard 184) coated hanging-drop microslides were used. The cavities on the slide were filled with 250 μL of mineral oil. Then, in the case of microgel synthesis, 1 μL aqueous droplets containing monomers, comonomers, crosslinker, and photoinitiators were placed on the surface of mineral oil in each cavity. The photopolymerization was initiated by irradiation with UV light for 1 h, with the final product a spherical hydrogel 500 μm in diameter, floating on the surface of the mineral oil.

The synthesis of PNIPAm-based microgels and microcapsules were accomplished using w/o and o/w/o emulsions, respectively. In the case of the microcapsules' synthesis, the same procedure as described above was used, except that the droplets of an o/w emulsion were used in place of a monomer solution. The o/w emulsion comprises of silicone oil that is vigorously mixed-in with the same aqueous solution that is used for microgel synthesis.

In Table 1, the differences between the microgel and microcapsule structure are shown. The *microgel* possesses a crosslinked network of polymer throughout the hydrogel (presented in green). On the other hand, the *microcapsule*, in this study, features multicore–shell morphology. Multiple microdomains of silicone oil (presented in red) form small compartments within the crosslinked polymer shell. This morphology was consistent with the theoretically expected morphology from spreading coefficient calculations.[24] We previously demonstrated that when the encapsulated oil droplets were expelled above the VPTT of the polymer, hollow cores remained, which could be refilled by swelling with water-soluble drugs.

2.2 Characterization

2.2.1 Polymer morphology of microgels and microcapsules.
A detailed investigation of the microcapsule morphology was reported previously.[24] In the present study the morphology of both microgel and microcapsule samples was characterized using a laser scanning confocal microscopy (LSCM) (Fluoview 300, Olympus). In short, LSCM equipped with a digital camera (DP7, Olympus) allowed real-time observation of the hydrogels. A fluorescent dye, FITC, was added to the aqueous phase containing monomer droplets as they polymerized into hydrogel microspheres and eventually into either microgels or microcapsules depending on the system. In the case of the microcapsule, Rhodamine B dye was added to silicone oil enabling visualization of the multi-cores in the inner structure of the microcapsules. The samples were observed under the LSCM, using an excitation wavelength of 488 nm for FITC dye (which labeled the polymer in the microgels and microcapsules) and 543 nm for Rhodamine dye (which was incorporated in the oil cores of the microcapsules). Note that these fluorescent dyes were used only for the morphology study. They were omitted in all other experiments.

2.2.2 Water uptake.
Thermal Gravimetric Analyzer (TGA) was used to determine the amount of aqueous solution taken up by the hydrogel particles. As shown in Scheme 2, the weight of ten cleaned and dried microgels or microcapsules were determined using the highly sensitive analytical balance in the TGA. The samples were then placed in DI water for at least 3 h to allow the particles to reach their maximum swelling capacity. The loaded particles were then reweighed again. They were then dehydrated in the TGA at a constant temperature, 60 °C until a constant weight was obtained. The results reported were averages of three replicates.

The water uptake is calculated from the difference in weight of the fully hydrated hydrogel (W_h) and dried particles (W_d), as shown:

$$\text{water uptake (\%)} = \left(\frac{W_h - W_d}{W_d} \right) \times 100 \qquad (1)$$

2.2.3 Drug loading efficiency.
The amount of the FITC–dextran loaded inside the microparticles was determined by TGA. Dried microgels or microcapsules were weighed using a

Table 1 A comparison of the microgel's and microcapsule's morphologies and properties

Morphology	Synthesis	Advantages	Disadvantages
Microgel	• Two-phase, water-in-oil emulsion (w/o)	• Simple and easy to synthesize • Drug can be reloaded multiple times	• Can only be used for water-soluble drug
Microcapsule	• Three-phase, oil-in-water-in-oil double emulsion (o/w/o)	• Can be used for water soluble drug alone or water and oil soluble drugs at once	• Uniformity of core sizes
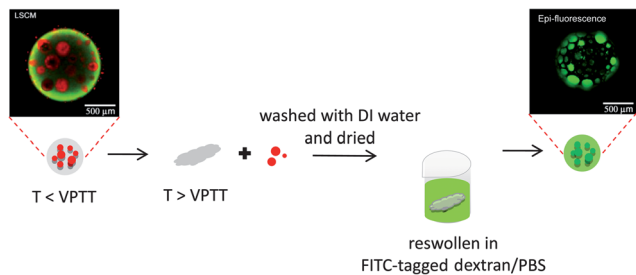
Scheme 2 Illustration of the loading process used in water uptake experiments and release kinetics studies. The schematic illustrates a microcapsule loaded with FITC–dextran in PBS solution. The red droplets in the cores represent silicone oil dyed with Rhodamine B. The green droplets in the cores represent FITC–dextran which is used as a model water-soluble drug. Photos are actual LSCM images of the corresponding microcapsules.

TGA before placing into a FITC–dextran solution ($1 \, mg \, mL^{-1}$) and incubated for 24 h. The fully swollen microparticles were then separated from the solution. They were then added to 1000 μL of DI water and heated to 50 °C for 5 min to eject and release the FITC–dextran. The amount of drug released into the supernatant was quantified by taking the difference between the loaded hydrogel and the dried weight of the hydrogel.

The amount of model drug loaded in hydrogel particle or loading efficiency is determined using the equation below:

$$\text{loading efficiency} = \frac{\text{amount of drug loaded in the particle in } (\mu g)}{\text{dried weight of the hydrogel particles } (mg)}$$
(2)

2.2.4 *In vitro* drug release experiment. The effect of morphology (*i.e.* microgel or microcapsule) on the drug loading and release kinetics of a model water-soluble drug FITC–dextran was studied in PNIPAm-based microgels and microcapsules. LSCM was used to monitor the amount of drug released at 25, 37, and 45 °C. A FITC–dextran loaded hydrogel was placed in a cavity on a hanging-drop microslide. The cavity was then filled with 150 μL of DI water. A warm stage (WS50-STC20A, Instec) was used to maintain a constant temperature. The amount of the drug released into the supernatant at a given time was determined by measuring the fluorescence intensity of FITC–dextran ($\lambda_{ex} = 490$ nm and $\lambda_{em} = 520$ nm) in the aqueous solution surrounding the microgel particles. The fluorescence intensity was manually measured from images acquired every 5 min using the intensity measurement feature in the microscope's FluoView software. A calibration curve prepared by measuring the intensities of known concentrations was used to determine the concentration of the released drug. The standard curve illustrating a linear relationship between FITC–dextran concentration and fluorescent intensity at 520 nm is shown in Fig. S1.† The results reported here are normalized and converted to percent cumulative release.

3 Results and discussions

We previously reported the effect of PEGylation on the temperature response, protein adsorption,[29] and mechanical properties[35]

of crosslinked PNIPAm hydrogels. There is a significant influence of the presence of PEG, its molecular weight (M_n 300 and 1100 g mol^{-1}) and its concentration (10, 20, and 30 wt%) on the value and breath of the VPTT, the protein adsorption, and the mechanical response of the hydrogels. 20 wt% and M_n 300 g mol^{-1} PEGMa was the critical concentration and molecular weight in the copolymer that minimized protein adsorption while optimizing the balance between mechanical strength and flexibility. Hence, in the current study, PEGMa is incorporated at 20 wt% and a M_n 300 g mol^{-1} was used to prepare PNIPAm-*co*-PEGMa microgels and microcapsules. The results in this study is reported here by considering first, the effect of the polymer type and then second, the effect of morphology on the release kinetics of the model drug, FITC–dextran.

3.1 Effect of polymer morphology on water uptake

Knowledge of the equilibrium degree of swelling allows for the calculation of polymer network parameters, such as the distance between crosslinks and the pore size of the hydrogel. For PNIPAm-based microgels, the initial water uptake after 24 h incubation in DI water at 25 °C is shown in Fig. 1. The water uptake followed the trend of PEGMa > PNIPAm-*co*-PEGMa > PNIPAm for both microgels and microcapsules. It was observed that the water uptake of PNIPAm microgel is approximately 300 wt%, the lowest of all three polymers. PEGMa microgel gave the highest water uptake of ~500 wt%. This result is expected as PEGMa is more hydrophilic than PNIPAm. Also, due to the bulkier PEG macromonomer (M_n 300 g mol^{-1}), it is assumed that the space between crosslinks or pore size in the PEG microgels is significantly larger than that of the PNIPAm microgel. We confirmed this assumption by calculating the relative pore sizes, reported in the next section. Based on this higher water uptake and larger expected pore size in PEGMa, we hypothesized that the drug release rate for PEGMa microgels will be greater than that of PNIPAm microgels for a diffusion-controlled release mechanism.

For the microgel comprising of the copolymer, PNIPAm-*co*-PEGMa (20 wt%), the water uptake is around 400%, which is expected, as incorporating PEGMa into PNIPAm increases its hydrophilicity. Lee and Lin reported similar results using HEMA-*co*-PEGMa hydrogels.[36] The pore size or volume between crosslinks for the copolymer is expected to be in between that of PNIPAm and PEG.

When the morphology of the hydrogel is changed from a microgel to a microcapsule, the water uptake is increased for all polymer compositions. This increase in water uptake is in the range of 30–50%. This result indicates that having hollow multi-cores within the microcapsules, increase their loading capacities. This is potentially beneficial for high-dose drug delivery applications.

3.2 Effect of polymer morphology on drug loading capacity

The loading efficiency of the microgels and microcapsules is shown in Fig. 2. The loading efficiency of PNIPAm and its copolymer PNIPAm-*co*-PEGMa (20 wt%) microgel is approximately 2 μg FITC–dextran per mg dried hydrogel. In contrast, it
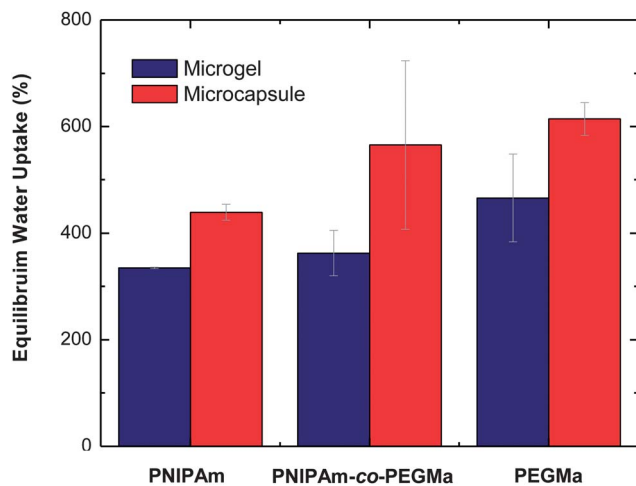
Fig. 1 Equilibrium water uptake in wt% of PNIPAm, PEGMa, and PNIPAm-*co*-PEGMa (20 wt%) microgels and microcapsules after 24 h incubation in DI water at 25 °C.

increases three-fold to ∼6.5 µg FITC–dextran per mg dried hydrogel in PEGMa microgels. This may be due to two factors; the relative swelling ratio (obtained from the water uptake above) and the pore sizes.

The water uptake result is in direct correlation with the loading efficiency results. That is, PNIPAm-*co*-PEGMa (20 wt%) shows almost equal water uptake as that of PNIPAm, and it is less than that of PEGMa.

The calculated pore sizes (described in the next section) show that they are large in PEGMa (130 Å) while PNIPAm and the copolymer, PNIPAm-*co*-PEGMa (20 wt%) possess pore sizes of 78 Å and 92 Å, respectively compared to the corresponding microgel. A larger pore size will facilitate (FITC–dextran hydrodynamic radius is 58 Å) easy diffusion of the drug in and out because of a shorter tortuous path as compared to hydrogels with smaller pore sizes.

The role of particle morphology was also found to be significant. There is an increase in loading efficiency in the
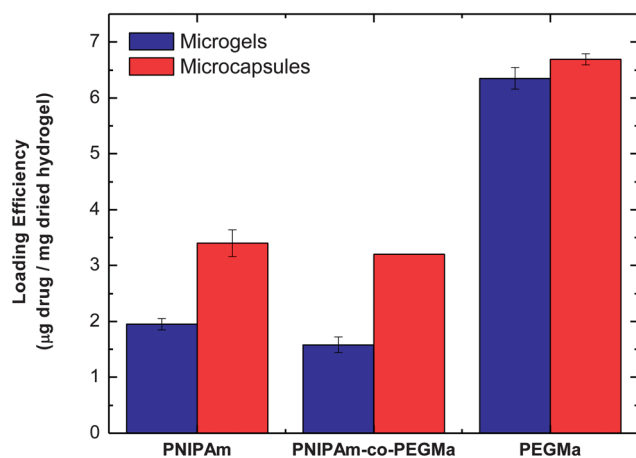

Fig. 2 Loading efficiency of FITC–dextran into microgels and microcapsules of PNIPAm, PNIPAm-*co*-PEGMa (20 wt%), and PEGMa. The data is an averaged value of three replicates and the error bars represent the standard deviation.

microcapsule of PNIPAm and PNIPAm-*co*-PEGMa (20 wt%) of 75 and 100%, respectively. In comparison, the increase in loading efficiency is not significant in the PEGMa microcapsule (∼5%). This result implies that the hollow cores created by the double emulsification process increases the free volume in the PNIPAm and PNIPAm-*co*-PEGMa (20 wt%). The increase in free volume in PEGMa however, is insignificant in comparison to the large free volume already present due to its large pore size (130 Å).

3.3 Calculation of polymer network parameters (porosity and M_c)

The three important parameters for structural characterization of swollen gels are the swelling factor Q, the average molecular weight between cross-links M_c, and the network pore size, ξ. An illustration of the M_c and ξ in a swollen hydrogel is shown in Scheme 3.

The swelling factor, Q represents the ratio of the volume of swollen gel V_s, and the polymer volume V_p. It also equals the reciprocal of the polymer volume fraction in the swollen gel $v_{2,s}$:

$$Q = \frac{V_s}{V_p} = \frac{1}{v_{2,s}} \tag{3}$$

Highly cross-linked networks exhibit lower swelling than loosely cross-linked networks and thus have smaller swelling factors. M_c represents the molecular weight of polymer chains between neighboring junctions as shown in Scheme 3. The network mesh or pore size, ξ, determines the average distance between crosslink points in the gel and thereby, the degree of gel porosity. With respect to their pore size, hydrogels can be divided into macroporous, microporous or nonporous gels. The higher the cross-link density, the smaller M_c and pore sizes are. The swelling factor can be determined experimentally by swelling measurements and allows the calculation of M_c and pore size.

The average pore size, ξ of a network can be related to M_c as shown:

$$\xi = v_{2,s}^{-\frac{1}{3}} l \left(\frac{C_n 2 \bar{M}_c}{M_r} \right)^{\frac{1}{2}} \tag{4}$$

where C_n is Flory characteristic ratio which is a constant for a given polymer–solvent system. C_n of PNIPAm is 11.7 and PEG is 3.8. l is the carbon–carbon bond length for vinyl polymers taken as 1.54 Å.

The molecular weight between crosslinks, M_c was calculated using Flory's equations.[37] This equation was later applied by Lu and Anseth[38] for evaluation of M_c values in PEG-based networks:
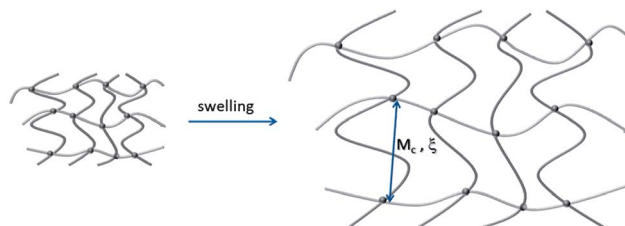
Scheme 3 Illustration of swelling in a hydrogel comprised of crosslinked polymer chains in the presence of water.

$$\frac{1}{\overline{M}_c} = \frac{2}{\overline{M}_n} - \frac{(\overline{v}/V_1)\left(\ln(1 - v_{2,s}) + v_{2,s} + \chi v_{2,s}{}^2\right)}{v_{2,r}\left(\left[\dfrac{v_{2,s}}{v_{2,r}}\right]^{\frac{1}{3}} - \dfrac{1}{2}\left[\dfrac{v_{2,s}}{v_{2,r}}\right]\right)} \qquad (5)$$

where M_n is the number-average molecular weight of the polymer before cross-linking, $\overline{v}$ is the specific volume of the polymer (reciprocal of its density), V_1 the molar volume of the water (18 cm^3 mol^{-1}), $v_{2,r}$ is defined as the polymer volume fraction after crosslinking but before swelling (the relaxed polymer volume fraction), $v_{2,s}$ is the polymer volume fraction after equilibrium swelling (swollen polymer volume fraction), and χ the Flory–Huggins polymer–solvent interaction parameter.[39] The calculated values of the swelling factor, Q, average end-to-end-distances M_c, and pore sizes, ξ are given in Table 2. The swelling factor of PNIPAm and the copolymer were found to be similar, whilst PEGMa had a swelling factor 1.5 times greater. It should be noted that, when the amount of water is higher than its maximum swelling amount, the water-phase coexists with the hydrogel-phase.

The value of the pore size, ξ, for these networks should be taken as an order of magnitude estimate, as it shows that in the PNIPAm network, the pore size is of the same order of magnitude as the size of the FITC–dextran molecule.

Specifically, from Table 2, it can be seen that PNIPAm possesses the smallest pore size of 78.78 Å which is smaller than that of the copolymer PNIPAm-*co*-PEGMa (20 wt% PEGMa) (ξ = 92.64 Å), and almost two times smaller than that of PEGMa (ξ = 130.92 Å). These results are in agreement with pore sizes determined previously by the authors *via* cryogenic-SEM.[35] This result indicates that the PNIPAm network is denser than that of PEGMa and the copolymer. Therefore, we hypothesize that the diffusion of FITC–dextran will follow the trend PEGMa > PNIPAm-*co*-PEGMa > PNIPAm. Also, based on the pore size, the investigated hydrogels can be regarded as microporous.[40]

3.4 Release kinetics of PNIPAm-based microgels

Monitoring the release of dextran was accomplished using FITC-tagged-dextran together with LSCM, with an excitation wavelength of 488 nm and an emission wavelength of 520 nm. When a proper photomultiplier or PMT setting is used, FITC–dextran intensity is linearly related to its concentration. In Fig. 3 a set of LSCM images of FITC–dextran released from PNIPAm microgels into the surrounding DI water (constant volume of 150 μL) at 45 °C, is shown. The intensity profile can be deduced from a straight line drawn across an image from the left to right (white line). The intensity at a fixed position was used to monitor the change in intensity over time. The position of 1000 μm was chosen because it allowed observation of the drug release from the microgel over the chosen time period and enabled distinction between slow release and burst release behavior.

Fig. 4 illustrates the release of the model drug from PNIPAm-based microgels at constant temperatures of 25, 37, and 45 °C over the course of 3 h as well as the plot of released drug intensity as a function of time and temperature. At 25 °C, which is below the VPTT of PNIPAm, the drug release is mainly controlled by the chemical potential difference between the inside of the microgel network and the DI water surrounding the microgel. The release profile of PNIPAm showed an initial slow release followed by a sudden increase in rate which may suggest the release does not follow first order kinetics and there are other mechanisms involved in the release kinetics other than a diffusion mechanism. The graphs illustrating that the release does not follow first order kinetics is shown in Fig. S2. In fact, the initial slow release indicates the presence of a surface resistance on the microgel. This inhibition in the release behavior has not been observed by others[2,36] for example, when caffeine (M_w 197 g mol^{-1}), vitamin B12 (M_w 1355 g mol^{-1}), or crystal violet (M_w 407 g mol^{-1}) were studied. A plausible explanation may be that the drug model molecule (FITC–dextran, 70 kDa) is relatively large (Stokes radius, 58 Å), compared to the PNIPAm pore size, whereas this is not the case for caffeine, vitamin B12, or crystal violet.

The release of the model drug became faster as the temperatures were increased to the VPTT of PNIPAm, from 25 to 37 °C and then to that above VPTT at 45 °C. The initial release rates seen from the initial release profile in Fig. 4 (<60% or <30 min) indicated that the release rate increases exponentially with temperature in PNIPAm. At 45 °C, the release ultimately reaches its equilibrium after 120 min. The faster rate at T > VPTT may be as a result of a combination of a "*squeezing*" mechanism due to a bulk network collapse[41] and an increasing of the system's kinetic energy coupled with chemical potential diffusion.

A plausible explanation for these results is that the PNIPAm network deswelling caused a decrease in the free volume in the microgel, causing the loaded drug to be released from the PNIPAm microgel at a faster rate. Hoffman indicated[2] that the release at T > VPTT is a very complex process for PNIPAm hydrogels. The release process starts with a temperature gradient across the gel and in the first few seconds, a burst of surface drug accompanies the formation of a dense "*skin*" and a buildup of hydrostatic pressure inside the gel. This pressure will tend to "*squeeze*" out the fluid containing the drug as the polymer collapses. Molecular diffusion processes will occur in parallel.

It is interesting to note that temperatures at or above the LCST, the release kinetics of PNIPAm have been were reported to be either slower[26,42] or faster[41] by different studies. In fact, the release kinetics depends on which step in the release process dominates the release behavior for a particular system. For example, a slower release rate as temperature increases to or above VPTT would indicate a greater resistance to diffusion due to a "*skin-effect*" and faster release rate[41] would indicate a bulk deswelling, as explained previously.[43]

Table 2 Calculated average network pore size, (ξ) for the microgels

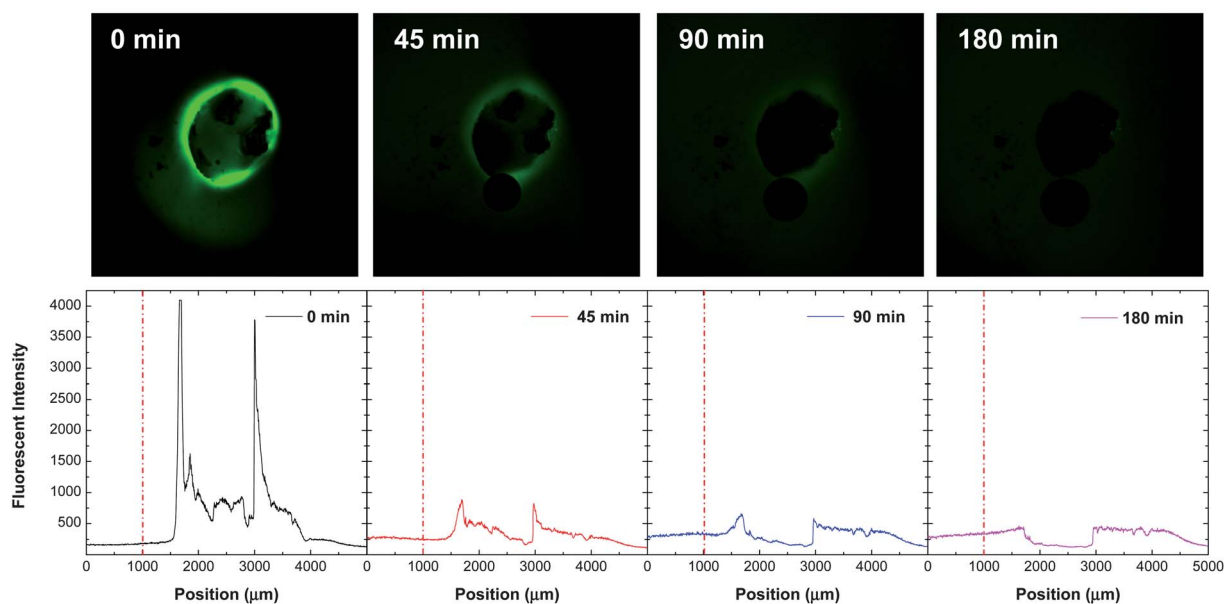| Microgels	Q	M_c (g mol^{-1})	Pore size (ξ, Å)
PNIPAm	3.35	56.58	78.78
PEGMa (M_n 300 g mol^{-1})	4.66	150.00	130.92
PNIPAm-*co*-PEG (20 wt% of PEGMa, M_n 300 g mol^{-1})	3.63	75.26	92.64

Fig. 3 Representative intensity profiles of FITC–dextran released from PNIPAm-based microgels measured at 45 °C, over a 3 h period. The amount of FITC–dextran loaded is measured by the difference in fluorescence between a solution of FITC–dextran at the same concentration of that mixed with PNIPAm-based microgels and FITC–dextran left in the supernatant.

Comparing the release rate of PEGMa with PNIPAm microgels at 25 °C, the release rate of PEGMa microgels was found to be faster than that of PNIPAm microgels, as predicted previously from the water uptake and loading capacity results. PEGMa microgels do not possess a VPTT in the testing range. Therefore, the release profiles suggest that a diffusion mechanism play a major role in the drug release in this case. Note that at all three temperatures, drug release reaches its equilibrium in less than 100 min, faster than in the case of PNIPAm microgels at any temperature. The release rate of FITC–dextran in PEGMa microgels becomes slightly faster as the temperature increases which may be due to the system's kinetic energy and polymer chain relaxation.

A plausible explanation for these results is as follows. In the current experiments during diffusion-controlled release ($T <$ VPTT), FITC–dextran travels through a large pore size PEGMa network ($\xi = 130$ Å), with ease and experience very little resistance to diffusion from the polymer network. In comparison, the denser network of PNIPAm ($\xi = 78$ Å), provides a much greater resistance to diffusion; the molecules need to find the path of least resistance so the denser network of PNIPAm lengthens the exit path for the drug molecule. As a result, the diffusion rate in PNIPAm is slower than in PEGMa.

In the case of the copolymer, PNIPAm-*co*-PEGMa (20 wt%) microgels having a pore size of 92 Å, the release kinetics of FITC–dextran is significantly faster than that in PNIPAm microgels. In fact, the initial release rates at 25 °C and 37 °C are closer to that of PEGMa than that of PNIPAm. This implies that PEGMa dominates the initial release behavior at $T <$ VPTT. Similar results have been reported by Lee and Lin, that is, incorporating PEGMa into HEMA hydrogels also increases their diffusion coefficient and the penetration velocity of water through the hydrogel.[36]

The release behavior of PNIPAm-*co*-PEGMa (20 wt%) microgels, at 45 °C is significantly different. At 45 °C, which is close to the VPTT of the copolymer,[24] a stepwise release profile was observed. The initial release rate was significantly inhibited before a *short burst-release* took place, followed by a rather subtle set of *slow-then-burst* release cycles. This stepwise release near the VPTT of the copolymer indicates heterogeneity of the copolymer network. A plausible explanation is that PNIPAm-rich microdomains have been formed, and they were responsible for the fast release step, whereas the PEGMa-rich microdomains were responsible for the initial inhibition period.

The inhomogeneous nature of copolymer microgels synthesized by free radical polymerization has been reported by various research groups. It has been shown[44–46] that the comonomers as well as the cross-linker distributions within PNIPAm microgels particles are, in general, heterogeneous. McPhee *et al.*,[47] reported that the cross-link density decreases from the center to the periphery because of the difference in reactivity ratios of the comonomers. Alava and Saunders,[48] reported on the reactivity ratios of the same polymers used in the current study. The reported values are $r_{NIPAm} = 1.2$ and $r_{PEGMa} = 0.13$. These reactivity ratios suggest that PNIPAm-rich regions could be formed, which inevitably results in phase separation. From this information one can legitimately hypothesize that PNIPAm-rich microdomains in PEG-rich regions may be formed as well during polymerization.

3.5 Effect of hydrogel pore size on release kinetics

To gain further insight into the interesting release profiles for the microgels, the effect of gel pore size on FITC–dextran release was examined. The results presented in Fig. 4 and 5, suggest that in general, there is a correlation between the gel pore size
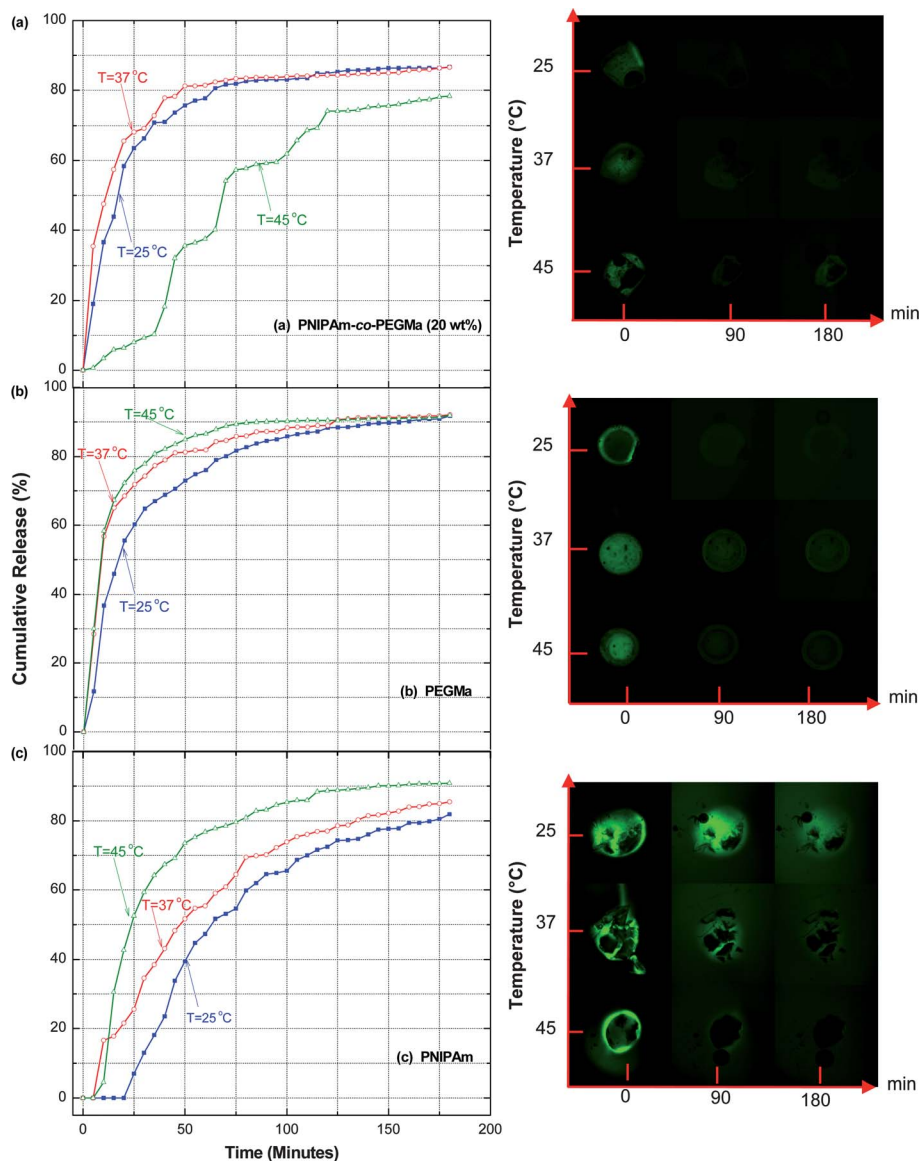
Fig. 4 Normalized average cumulative release profiles *versus* time of FITC–dextran from PNIPAm-based microgels at 25, 37, and 45 °C. The fluorescent images represent drug release from (a) PNIPAm-*co*-PEGMa (20 wt%), (b) PEGMa and (c) PNIPAm microgels at different temperatures *versus* time.

and the global release profile. Since diffusion of the solute occurs through the open spaces between the polymer chains, the release rate of FITC–dextran is expected to be lowered as the pore size is decreased. This was found to be exactly the case in the current study. Due to the larger pore size of PEGMa hydrogels, encapsulated FITC–dextran can rapidly diffuse out of the network in consequence of their size, 58 Å. In fact, FITC–dextran was almost totally released at an early stage for PEGMa and the copolymer compared to the PNIPAm hydrogel, regardless of temperature, with the exception of the copolymer at $T >$ VPTT. The latter behavior will be explained in the next section.

3.6 Effect of polymer morphology on release kinetics

The effect of particle morphology on the release behavior of PNIPAm, PEGMa, and PNIPAm-*co*-PEGMa (20 wt%) microgels

and microcapsules at 25, 37, and 45 °C is shown in Fig. 5. In general, the release of FITC–dextran from microcapsules (red) is faster than that from microgels (blue). A stepwise release profile from PNIPAm microcapsules is found in most cases where the temperature is below the VPTT and also in PEGMa microcapsules (which do not possess a VPTT). This result provides evidence to our hypothesis that an inhomogeneous structure may yield a stepwise release behavior as is observed in the case of PNIPAm-*co*-PEGMa microgels.

The presence of multiple cores in a hydrogel to form multi-core microcapsules is one way to introduce another mechanism for drug release, *i.e.* osmosis. A thin film of the hydrogel dividing each liquid-filled core acts as a semipermeable membrane. Once diffusion release begins, the solute concentration on both sides of the membrane becomes out of balance, and as a consequence, an osmotic transport mechanism occurs. The
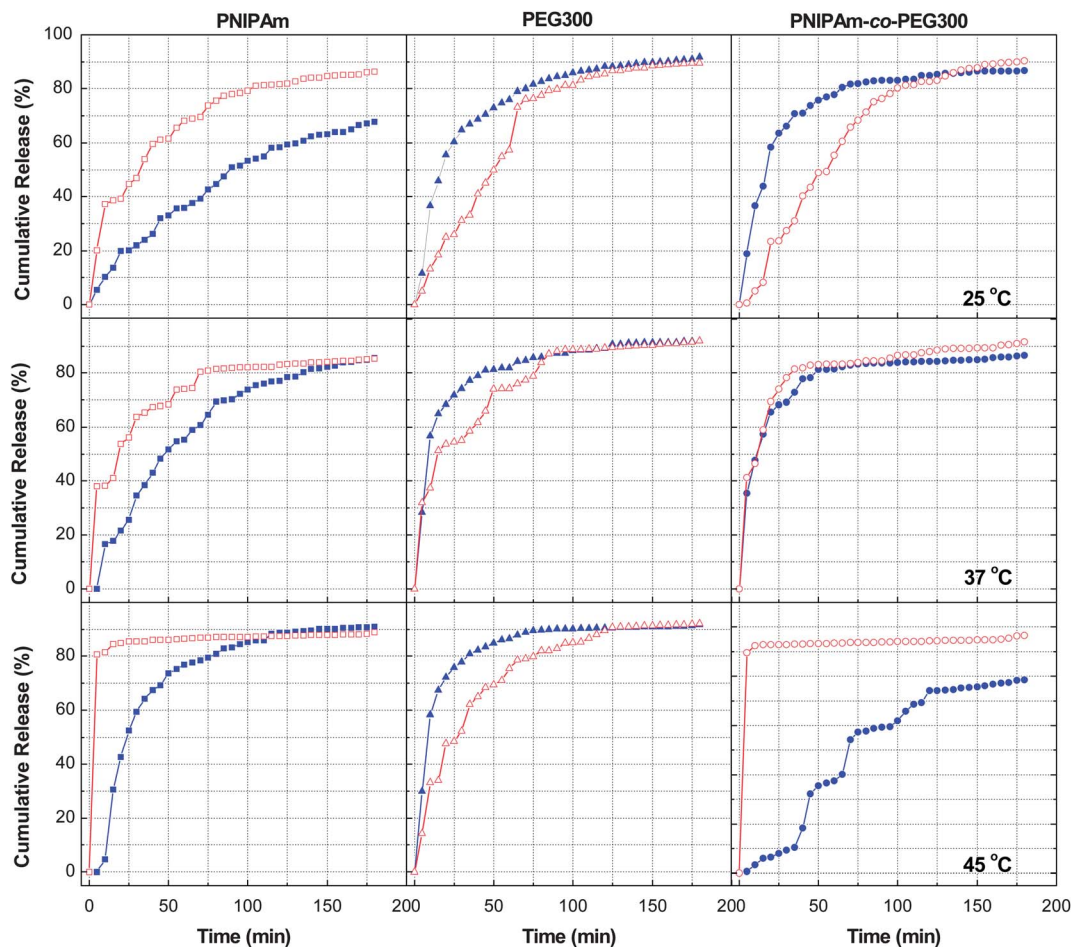
Fig. 5 The effect of hydrogel morphology on the release kinetics of FITC–dextran at different temperatures is shown. The results indicate that the release rate from microcapsules (red) is in general, faster than that from microgels (blue).

release mechanism for a multicore-microcapsule system is indeed a very complicated process. Osmotic transport takes place immediately once the diffusion mechanism starts. Therefore, the aim is to equalize the solute concentrations on the outside and inside of the particle. Once the osmotic balance between the hollow cores next to the particle surface and the ones close to the particle center are out of balance another sequence of osmosis is triggered. A series of osmotic transport phenomena can occur as described, until the concentrations in the center and outside of the microcapsule reach equilibrium. Recall, that this domino effect of osmotic transportation take places concurrently with the diffusion mechanism controlled by the polymers' matrix properties, as described in the microgel section above (Section 3.4). The exact size of the step–release profile of the microcapsules may depend on the number and size of the cores and the distance between them. Further investigations of these parameters will be reported in the future, as the authors are currently working on precisely controlling the number and size of the cores in the microcapsules by conducting the double emulsion synthesis using a microfluidic device.

At 45 °C (> VPTT), burst release was observed in both the case of PNIPAm and its copolymer PNIPAm-co-PEGMa (20 wt%). This burst release is due to a large hydrostatic pressure build-up in

the hollow cores as the deswelling of the hydrogel network takes place. This result implies that incorporating hollow cores (which can be filled with liquid containing drugs) in microcapsules can be used to ensure burst release delivery will be achieved with thermal stimulation.

Overall, these results reveal that PEGylated PNIPAm hydrogels may be used for controlled delivery of a water-soluble drug for an extended period of time by adjusting the copolymer composition, morphology, and pore size.

3.7 Temperature dependence of diffusion coefficient

In order to understand the precise mechanism of drug release from the hydrogels Peppas et al.,[33,49] developed an empirical equation, termed the power-law model as shown in eqn (6). This equation can be used at initial release times (initial 60% of drug release) to identify the mechanism of release as a function of time for a given geometry, as detailed in Table 3:

$$\frac{M_t}{M_\infty} = kt^n \tag{6}$$

where M_t is the total cumulative mass of drug released at time t, M_∞ is the total cumulative mass of drug released at infinite time

(equilibrium), M_t/M_∞ represents the fractional release of the drug with respect to the value at infinite time, k is a constant related to the diffusion coefficient, and n is the diffusional exponent reflecting the specific transport mechanism.

This power law equation is used to account for the coupled effects of Fickian diffusion and viscoelastic relaxation in polymer systems. Transport in swelling systems can be described by Fick's second law, with *diffusion dependent on concentration gradients*.

3.7.1 Fick's first law. The release of an active agent from a polymeric controlled release device consists of the movement of the drug trough the bulk of the polymer. This phenomenon, known as diffusion, is to a large degree controlled by the mass-transfer limitations at the boundary between the polymer carrier and its surroundings. On a macroscopic level, the transport or release of a drug through a polymeric controlled release device can be described by Fick's classical diffusion theory.[50,51]

Fick's first law governs the steady-state diffusion circumstance:

$$J = -D\frac{dc}{dx} \tag{7}$$

where J is the molar flux of the drug (mol cm^{-2} s^{-1}), c is the concentration of drug, D is the diffusion coefficient of the drug in the polymer and x represents the distance diffused in time, t. It should be noted that the diffusion coefficient is assumed to be independent of concentration.

3.7.2 Fick's second law. For many drug delivery devices, the release rate will be time dependent. Fick's 2nd law controls the unsteady state and is used to analyze the release behavior (which can be derived from Fick's 1st law and mass balance considerations) and it predicts how diffusion causes the concentration to change with time:

$$\frac{\partial C}{\partial t} = \frac{\partial}{\partial x}\left(D\frac{\partial c}{\partial x}\right) \quad \text{or} \quad \frac{\partial C}{\partial t} = D\frac{\partial^2 C}{\partial x^2} \tag{8}$$

where D is the diffusion coefficient or diffusivity in dimensions of length^2 time^{-1}, C (for ideal mixtures) is the concentration in dimensions of amount of substance length^{-3}, in units mol m^{-3}, χ is the position (length), t is time with boundary and initial conditions given below:

$$\text{at } t = 0, C(x,t) = C_0$$

$$\text{at } x = \delta(t), C = C_b$$

$\delta(t)$, represents the distance from the center of the sample to the surface, which increases with time due to polymer swelling. C_b represents the bulk concentration at the surface of the polymers, usually treated as zero under perfect sink conditions:

$$\text{at } x = 0, \quad \frac{\partial C}{\partial x} = 0$$

The second law can thus be solved to give:

$$\frac{M_t}{M_\infty} = 4\left[\frac{Dt}{l^2}\right]^{\frac{1}{2}}\left[\frac{1}{\pi^{\frac{1}{2}}} + 2\sum_{n=1}^{x}(-1)^n\text{ierfc}\left(\frac{nl}{2\sqrt{Dt}}\right)\right] \tag{9}$$

which at short times is reduced to:

$$\frac{M_t}{M_\infty} = 4\left[\frac{Dt}{\pi l^2}\right]^{\frac{1}{2}} \tag{10}$$

Eqn (10) leads to the square root of time dependence observed in Fickian diffusion. For the release that is measured by the intensity of a fluorescently tagged molecule, the mass fraction is replaced by fluorescence intensity fraction as shown below:

$$\frac{I_t}{I_\infty} = 4\left[\frac{Dt}{\pi l^2}\right]^{\frac{1}{2}} \tag{11}$$

Eqn (11) represents an approximate solution valid for describing short-time behavior for one-dimensional release from the microgels and microcapsules. To determine the diffusion coefficient at short times (t) we assume: (1) no swelling of the polymer takes place, and (2) the drug release is mainly due to its concentration difference. Thus, it can be assumed that the diffusion power law index, n is 0.5, when the boundary conditions are employed at small t, and l is constant.

In addition, since Fick's second law is based on uniform distribution of the drug in the device (cylinder or sphere), an indirect and qualitative assessment was made to investigate if the loaded hydrogels are homogeneous. Homogeneity was obtained from the LSCM images used to estimate fluorescence

Table 3 Diffusion coefficients deduced from the slope of fractional drug release *versus* square root of time shown in Fig. 6

Hydrogel	Temperature/°C	Microgel		Microcapsule	
		Diffusion/cm² s⁻¹ (1×10^{-6})	SD ($\pm$)/cm² s⁻¹ (1×10^{-6})	Diffusion/cm² s⁻¹ (1×10^{-6})	SD ($\pm$)/cm² s⁻¹ (1×10^{-6})
PNIPAm	25	0.53	0.01	0.67	0.00
	37	0.67	0.00	0.75	0.00
	45	1.31	0.01	12.16	0.00
PEGMa	25	0.92	0.01	0.58	0.00
	37	1.28	0.01	0.61	0.00
	45	1.77	0.02	0.56	0.00
PNIPAm-*co*-PEGMa	25	1.05	0.00	0.85	0.00
	37	1.29	0.01	1.67	0.01
	45	0.59	0.01	12.65	0.00

intensity. It is reasonable to assume based on the fairly uniform fluorescence from both the microgel and microcapsule alike, that the distribution of FITC–dextran in the respective polymer matrices is indeed uniform.

From eqn (11) a plot of fractional intensity of FITC–dextran release, $\frac{I_t}{I_\infty}$ versus $t^{1/2}$ gives the diffusion coefficient, D, as the slope. As seen in Fig. 6, the diffusion coefficient, D, of FITC–dextran was lower for PNIPAm than for PEGMa at 25 °C and for the microgels but not for the microcapsules. This may be due to temporary interactions between FITC–dextran and the polymer, the drug distribution and the non-ideal nature of the network. Temporary interactions may arise because FITC–dextran contains hydroxyl groups which may form temporary H-bonding with the amide groups of PNIPAm, slowing down its diffusion rate in the microgels but not in the microcapsules.

The experimental diffusion coefficients in relation to hydrogel composition and temperature are shown in Table 3. As will be discussed in Section 3.9 – *FITC–dextran release mechanism*, diffusion plays a dominate role in release in the microgels, but not the microcapsules, as such this is the reason for the reverse trend in diffusivity in the microcapsules for PNIPAm and PEGMa at 25 °C. It is important to note that as the temperature is increased to above the VPTT at 37 and 45 °C, the diffusion coefficients in PNIPAm microgels increase to 1.25 and 2.46 times that at 25 °C (T < VPTT), respectively.

The diffusion coefficient in microgels and microcapsules comprised of PNIPAm and its copolymer are temperature dependent but do not show a linear relationship in the Arrhenius plot as shown in Fig. 7 and 8. The diffusion in the microgels of the copolymer, however, decreased as the temperature approached its VPTT at ~45 °C. It is speculated that the shrinkage of PNIPAm-rich domains resulted in an inhibition of drug diffusion. The implications of this temperature dependent release will be discussed in more detail in Section 3.9.

In contrast, the diffusion of FITC–dextran in the microcapsule of the copolymer increase 12 times at T > VPTT compared to that at T < VPTT. This relatively large increase in the diffusion coefficient in the microcapsules is attributed to the presence of relatively large cores and the burst release brought on by the collapse of the polymer network due to the temperature responsiveness of PNIPAm. Note that while PEGMa microcapsules also possess relatively large cores, no dramatic increase in the diffusion coefficient is obtained with increasing temperature, because PEGMa is not temperature responsive.

Since diffusion of FITC–dextran occurs through the open spaces between the polymer chains, the release rate of the drug is expected to be lowered as the pore size is decreased. As expected, the experimentally calculated diffusion coefficient (Table 3) increased in direct proportion to the calculated pore size (Table 2). Indeed, this result is in agreement with trends reported previously in the literature.[52]
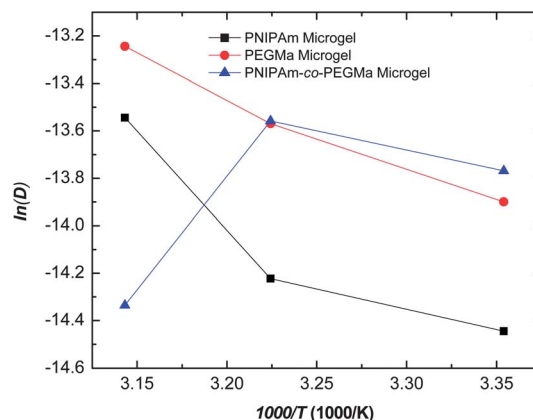

Fig. 7 Arrhenius plots of ln(D) of FITC–dextran *versus* the reciprocal of the absolute temperature in PNIPAm, PEGMa and PNIPAm-co-PEGMa (20 wt%) microgels.

Fig. 6 Fractional FITC–dextran release, I_t/I_∞ versus $t^{1/2}$ for release from microgels (filled symbols) and microcapsules (open symbols), at three different temperatures, 25, 37 and 45 °C.

Fig. 8 Arrhenius plots of ln(D) of FITC–dextran *versus* the reciprocal of the absolute temperature in PNIPAm, PEGMa and PNIPAm-*co*-PEGMa (20 wt%) microcapsules.
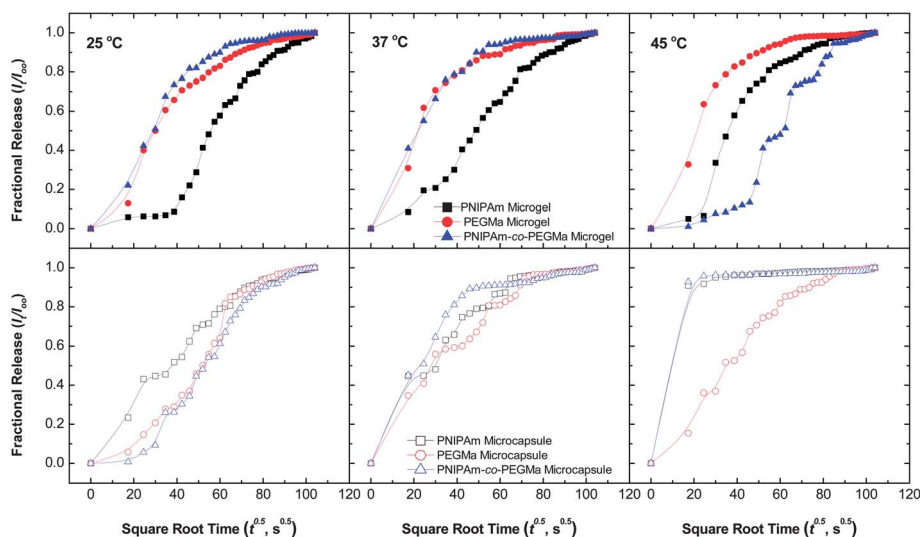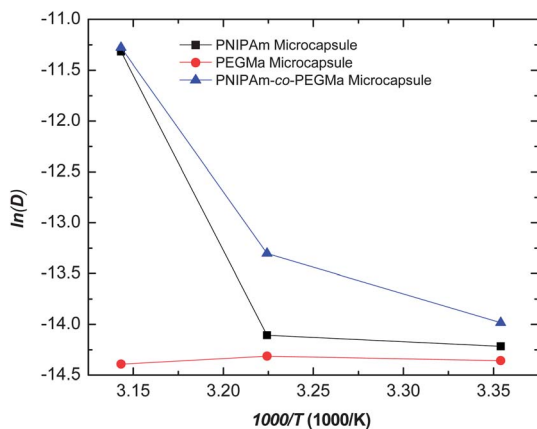
3.8 Activation energies obtained from the Arrhenius relationship

Diffusion through the hydrogel network can be interpreted as an activation process and the temperature dependence of the diffusion coefficients was fitted with an Arrhenius-type equation in order to determine the activation energies:

$$D = D_0 e^{-(E_a/RT)} \quad (12)$$

where D_0 represents the diffusivity at infinite temperature, T the absolute temperature, and E_a the activation energy.

3.8.1 Microgels. Fig. 7 presents the Arrhenius plots for FITC–dextran in the different microgels, PNIPAm, PEGMa, and PNIPAm-*co*-PEGMa (20 wt%). The Arrhenius plots of diffusivities are linear over the temperature range 25–45 °C for PEGMa microgels but PNIPAm and the copolymer shows a deviation in linear behavior. That is, release of FITC–dextran depends upon temperature (it becomes faster with an increase in temperature) for PEGMa microgels. The activation energy, E_a for FITC–dextran in PEGMa microgels was determined from the slope of the Arrhenius plot in Fig. 7 to be 25.44 kJ mol⁻¹. In contrast, the activation energies for PNIPAm and the copolymer could not be

determined because the diffusivity does not follow a linear relationship in the Arrhenius plot.

3.8.2 Microcapsules. The activation energy of PEGMa microcapsules is determined from the Arrhenius plot in Fig. 8 to be −0.99 kJ mol⁻¹. The negative value indicates that the release of FITC–dextran from PEGMa microcapsules is not affected by an increase in temperature. As was the case for the microgels, the activation energies of the microcapsules comprised of PNIPAm and the copolymer could not be determined because the diffusivity does not follow a linear relationship in the Arrhenius plot. In fact, the increase of diffusion coefficients of FITC–dextran in both microcapsules comprised of PNIPAm and its copolymer, by one magnitude at 45 °C indicates bursting of the microcapsule at this temperature. Therefore, in an attempt to elucidate the global release mechanisms for all the hydrogels, we will no longer consider the boundary conditions at short time (where the diffusional exponent is limited to 0.5). Consequently, the results of our investigation into the global drug release mechanisms of the hydrogels are presented in the next section.

3.9 FITC–dextran release mechanisms

The controlled release of FITC–dextran from PNIPAm-based microgels could be described by a combination of various mechanisms. The plot of fractional drug release *versus* $t^{1/2}$ in Fig. 6 suggests that Fickian's diffusion is not the main mechanism controlling drug release in PNIPAm-based microgels and microcapsules. As shown in Table 4, n is dependent on the geometry of the device as well as the physical mechanism of release.[33]

Fluorescent intensity measured by LSCM is directly proportional to the FITC–dextran concentration. Therefore, Peppas' approach[33,49] is applied to gain a fundamental understanding of the physical mechanisms controlling drug release from the microgels and microcapsules investigated in this study. Eqn (13) is the power-law equation using the fluorescent intensity of released FITC–dextran. I_t and I_∞ are fluorescent intensity measurements at time t and at equilibrium, respectively. The logarithm of eqn (13) is shown in eqn (14) and a plot of $\ln(I_t/I_\infty)$

Table 4 Mechanism of transport and diffusional exponent for polymer hydrogels

Type of transport	Diffusional exponent, n			Time dependence
	Slab or thin film	Cylinder	Sphere	
Case I: Fickian diffusion	0.5	0.45	0.43	$t^{1/2}$
Anomalous transport or non-Fickian transport, Fickian diffusion and polymer relaxation	$0.5 < n < 1$	$0.45 < n < 0.89$	$0.43 < n < 0.85$	t^{n-1}
Case II transport polymer relaxation or swelling-controlled	1	0.89	0.85	Time independent
Super case II transport	$n > 1$	$n > 0.89$	$n > 0.85$	t^{n-1}

vs. ln *t* can be made. A regression line was fitted to the linear part of the curve and the order of release is given by *n*, the slope and the *y*-intercept relates to the diffusional and structural characteristics of the hydrogel, (Fig. 9), respectively.

$$\frac{I_t}{I_\infty} = kt^n \tag{13}$$

$$\ln\left(\frac{I_t}{I_\infty}\right) = \ln k + n\ln t \tag{14}$$

The logarithmic diffusion of the three microgels at different temperatures is shown in Fig. 9. The calculated diffusion exponent, *n* is summarized in Table 5, along with the estimated correlation coefficient R^2.

By determining the diffusional exponent *n*, one can gain information about the physical mechanisms controlling drug release from a particular device.[33] When *n* has a value of *n* < 1 this indicates diffusion controlled release (so-called Fickian diffusion or Case I). Non-Fickian or anomalous transport is observed for 0.45 < *n* < 0.89, with a limiting case of Case II transport (zero-order release) for *n* = 0.89. Non-Fickian behavior and Case II transport are indicative of coupling of diffusional and relaxation mechanisms. Occasionally, values of *n* > 0.89 have been observed and are considered to be Super Case II transport.[33] This mechanism could result from increased plasticization at the relaxing boundary (gel layer), that is, when the surface resistance becomes more significant relative to the diffusion resistance.

Fickian diffusional release occurs by molecular diffusion of the drug due to a chemical potential gradient. For systems exhibiting Case II transport, the dominant mechanism for drug transport is due to *polymer relaxation* as the gel swells. These are also known as *swelling-controlled* release systems. Anomalous transport occurs due to a coupling of Fickian diffusion and polymer relaxation.

Super Case II-transport, is a modification of the Case II-type transport. The uptake is initially linear as a function of time, but at some time well into the absorption process the rate of uptake suddenly increases. An explanation for this behavior has challenged many.[53] Super Case II transport is found when a significant entry resistance is combined with a concentration-dependent diffusion coefficient (with a combination of absorption and desorption).

Based on the calculated diffusional exponents from Fig. 9, the mechanisms of drug transport in spherical microgels are found to be dependent on temperature. For PNIPAm, the mechanism changes from Super Case II transport to Anomalous transport and then back to Super Case II transport as the temperature increases from 25 to 37, and then to 45 °C, respectively. Super Case II transport indicates that there is some phenomenon taking place in addition to chemical potential diffusion or Fickian's diffusion. The initial instance of Super Case II transport in PNIPAm at 25 °C may be due to a slow desorption of FITC–dextran complexed with PNIPAm. FITC–dextran contains hydroxyl groups and may form temporary H-bonding with the amide groups of PNIPAm, slowing down its diffusion rate.

As temperature is increased to 37 and 45 °C, polymer chain relaxation dominates the release mechanism. The softening of the microgel at an elevated temperature (indicating polymer chain relaxation) was reported in a previous study by the authors.[35] The resistance to diffusion at 45 °C may come from both polymer chain restriction (a denser shrunken polymer) and the adsorption and desorption processes competing with an increase in kinetic energy, and with Fickian's diffusion.

In the case of PEGMa microgel, relaxation of the polymer chain plays an important role in controlling the drug release behavior. This was also found to be true when PEGMa was incorporated into PNIPAm. This result suggests that PEGMa dominates the release kinetics of PNIPAm-*co*-PEGMa (20 wt%)
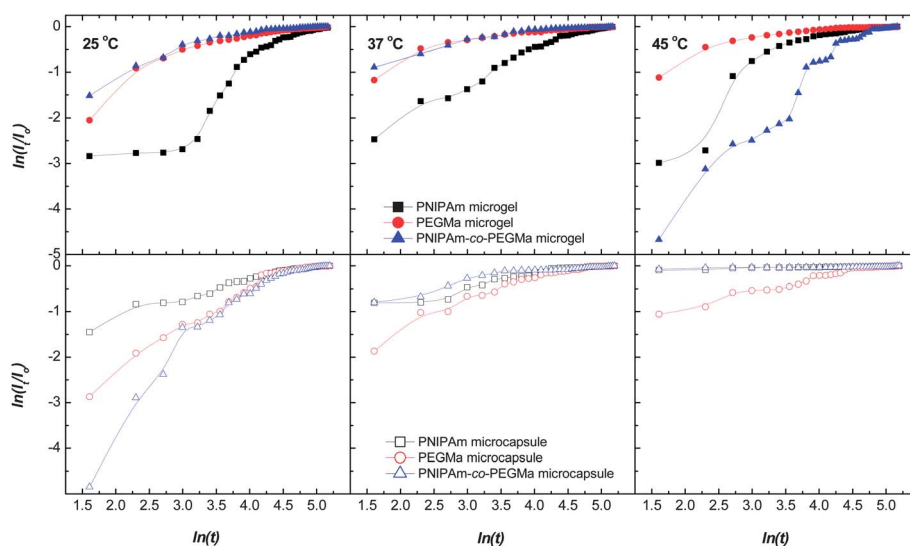

Fig. 9 FITC–dextran diffusion kinetics from PNIPAm, PEGMa, and PNIPAm-*co*-PEGMa (20 wt%) microgels (filled symbols) and microcapsules (open symbols) in DI water at 25, 37, and 45 °C.

Table 5 FITC–dextran diffusion mechanisms in PNIPAm, PEGMa, and PNIPAm-*co*-PEGMa (20 wt%) microgels and microcapsules in DI water at 25, 37, and 45 °C

Sample	Temperature (°C)	Microgel				Microcapsule		
		n	R^2	Mechanism		n	R^2	Mechanism
PNIPAm	25	1.17	0.86	Super Case II		0.45	0.96	Anomalous
	37	0.82	0.98	Anomalous		0.30	0.88	N/A
	45	1.55	0.89	Super Case II		0.03	0.96	N/A
PEGMa	25	1.00	0.90	Super Case II		0.93	0.99	Super Case II
	37	0.78	0.90	Anomalous		0.69	0.97	Anomalous
	45	0.76	0.92	Anomalous		0.33	0.97	N/A
PNIPAm-*co*-PEGMa	25	0.79	0.98	Anomalous		2.42	0.99	Super Case II
	37	0.44	1.00	Anomalous		0.39	0.98	N/A
	45	1.47	0.92	Super Case II		0.01	0.86	N/A

hydrogels when the temperature is at or below VPTT ($\leq$ 45 °C). Above VPTT however, the copolymer behavior is dominated by the release mechanism of PNIPAm. As a result, a drastic change in the release kinetics was observed as a function of temperature for the copolymer. In Table 5 for the corresponding microcapsule morphology at higher temperatures, N/A indicates that the release mechanism is not due to diffusion but instead a burst-release mechanism was observed.

4 Conclusions

The morphology and material composition of PNIPAm-based microgels and microcapsules greatly influence the release kinetics. Understanding the parameters that affect release kinetics is quite important for a variety of biomedical applications. PNIPAm microcapsules exhibit burst-release or pulse-release, which mimics chronobiological release of some regulatory agents such as hormones. An appealing advantage of the PNIPAm-*co*-PEGMa microcapsules is that the drug loading capacity can be quite high as facilitated by 30–50% increase in water uptake, compared to the corresponding microgel architecture. The presence of PEGMa increased the water uptake in both architectures due to its hydrophilic nature and its longer molecular weight between crosslinks (M_c). The estimated pore size for the PNIPAm, PNIPAm-*co*-PEGMa, and PEGMa hydrogels were 78, 92, and 130 Å, respectively.

In general, the release kinetics is dominated by polymer temperature responsiveness at $T >$ VPTT, and by hydrogel morphology at $T <$ VPPT. There is a striking advantage of using temperature responsive PNIPAm on the release kinetics. In fact, in microcapsules of both PNIPAm and its copolymer with PEG, a quick burst-release is observed at the stimulating temperature (45 °C which is $>$ VPTT). Specifically, more than 80% of the drug was released in the first 10 min using the temperature responsive microcapsule morphology, compared to 1 h for the corresponding microgel morphology.

The diffusion coefficients of the hydrogels were also estimated in an attempt to identify the release mechanisms. A deviation in the diffusivity plots at $T >$ VPTT for the thermoresponsive PNIPAm and copolymer hydrogels indicated that the drug transport was not *via* a diffusion release mechanism at $T >$ VPTT, but due to the bulk deswelling of the PNIPAm phase in the microgels and a burst-release mechanism in the

microcapsules. The release profiles from both microgels and microcapsules of PEGMa show a linear relationship in an Arrhenius plot. The activation energy of the PEGMa microgel was estimated to be 25.44 kJ mol^{-1} but a negative value was obtained for the corresponding microcapsule. In contrast, PNIPAm and the copolymer hydrogels gave a non-linear relation in an Arrhenius plot.

Although there is a correlation between the hydrogel pore size and the drug size, the mobility of the polymer chains as influenced by temperature, the extent of swelling and morphology (microgels or microcapsules) are factors that should also be taken into account in designing a polymeric drug delivery device. As expected, the experimentally calculated diffusion coefficient for PEGMa increased in direct proportion to the calculated pore size. Indeed, this result is in agreement with trends reported previously in the literature.[49,52,54,55]

Super Case II Fickian diffusion of FITC–dextran was observed for the PEGMa and copolymer microcapsules at $T <$ VPTT. Unlike some reports in the literature, the release of FITC–dextran is characteristic of a Super Case II and an Anomalous release mechanism for the copolymer microgels only when $T >$ VPTT and for the PNIPAm and PEGMa microgels only when $T <$ VPTT.

These results demonstrate the feasibility of modulating the release profile of encapsulated compounds by tailoring the polymer morphology and composition. Potential encapsulated compounds include proteins (for tissue repair), chemotherapeutics (for drug delivery) and nucleic acids (for gene delivery). These findings also illustrate the potential of the microcapsules' for co-delivery of drugs (hydrophilic and hydrophobic) and proteins or genes to improve the therapeutic efficacy in the treatment of diseases such as cancer due to the potential synergistic effect of targeted controlled multi-compound delivery and release. There is also the potential for using the different release mechanisms (*i.e.* diffusion (sustained) release and burst-release) in a single microcapsule device for controlled delivery of two different compounds.

References

1 H. G. Schild, *Prog. Polym. Sci.*, 1992, **17**, 163–249.
2 A. S. Hoffman, *J. Controlled Release*, 1987, **6**, 297–305.
3 A. S. Hoffman, *Macromol. Symp.*, 1995, **98**, 645–664.

4 H. Von Recum, A. Kikuchi, M. Okuhara, Y. Sakurai, T. Okano and S. Kim, *J. Biomater. Sci., Polym. Ed.*, 1998, **9**, 1241–1294.

5 E. Lee and H. Von Recum, *J. Biomed. Mater. Res., Part A*, 2010, **93**, 411–419.

6 Y. Matsumaru, A. Hyodo, T. Nose, S. Ito, T. Hirano and S. Ohashi, *J. Biomater. Sci., Polym. Ed.*, 1996, **7**, 795–804.

7 H. Yan and K. Tsujii, *Colloids Surf., B*, 2005, **46**, 142–146.

8 G.-H. Hsiue, S.-h. Hsu, C.-C. Yang, S.-H. Lee and I. K. Yang, *Biomaterials*, 2002, **23**, 457–462.

9 G. Huang, J. Gao, Z. Hu, J. St John, B. Ponder and D. Moro, *J. Controlled Release*, 2004, **94**, 303–314.

10 N. Milasinovic, M. Kalagasidis Krusic, Z. Knezevic-Jugovic and J. Filipovic, *Int. J. Pharm.*, 2010, **383**, 53–61.

11 R. Ramanan, P. Chellamuthu, L. Tang and K. Nguyen, *Biotechnol. Prog.*, 2006, **22**, 118–143.

12 A. Mathews, C.-S. Ha, W.-J. Cho and I. Kim, *Drug Delivery*, 2006, **13**, 245–251.

13 A. Afrassiabi, A. S. Hoffman and L. A. Cadwell, *J. Membr. Sci.*, 1987, **33**, 191–200.

14 N. Bertrand, J. Fleischer, K. Wasan and J.-C. Leroux, *Biomaterials*, 2009, **30**, 2598–3203.

15 J. Wu, B. Zhou and Z. Hu, *Phys. Rev. Lett.*, 2003, **90**, 048304.

16 C. Wu and X. Wang, *Phys. Rev. Lett.*, 1998, **80**, 4092–8186.

17 K. Plunkett, X. Zhu, J. Moore and D. Leckband, *Langmuir*, 2006, **22**, 4259–4325.

18 Y. Hirokawa and T. Tanaka, *J. Chem. Phys.*, 1984, **81**, 2.

19 S. Höfl, L. Zitzler, T. Hellweg, S. Herminghaus and F. Mugele, *Polymer*, 2007, **48**, 245–254.

20 D. Gan and L. A. Lyon, *Macromolecules*, 2002, **35**, 9634–9639.

21 I. K. Kwon and T. Matsuda, *Biomaterials*, 2006, **27**, 986–995.

22 K. H. Kim, J. Kim and W. H. Jo, *Polymer*, 2005, **46**, 2836–2840.

23 W.-F. Lee and Y.-H. Lin, *J. Mater. Sci.*, 2006, **41**, 7333–7340.

24 T. Trongsatitkul and B. M. Budhlall, *Langmuir*, 2011, **27**, 13468–13480.

25 C. M. Nolan, C. D. Reyes, J. D. Debord, A. J. Garcia and L. A. Lyon, *Biomacromolecules*, 2005, **6**, 2032–2039.

26 G. Fu and W. O. Soboyejo, *Mater. Sci. Eng., C*, 2010, **30**, 8–13.

27 D. E. Meyer, B. C. Shin, G. A. Kong, M. W. Dewhirst and A. Chilkoti, *J. Controlled Release*, 2001, **74**, 213–224.

28 S. R. Sershen, S. L. Westcott, N. J. Halas and J. L. West, *J. Biomed. Mater. Res.*, 2000, **51**, 293–298.

29 T. Trongsatitkul and B. M. Budhlall, *Colloids Surf., B*, 2013, **103**, 244–252.

30 C.-C. Lin and A. T. Metters, *Adv. Drug Delivery Rev.*, 2006, **58**, 1379–1408.

31 L. Wu and C. S. Brazel, *Ind. Eng. Chem. Res.*, 2008, **47**, 1518–1526.

32 J. Siepmann, A. Ainaoui, J. M. Vergnaud and R. Bodmeier, *J. Pharm. Sci.*, 1998, **87**, 827–832.

33 P. L. Ritger and N. A. Peppas, *J. Controlled Release*, 1987, **5**, 37–42.

34 *FITC–Dextran Technical Data Sheet*, TdB Consultancy AB, Virdings Allé 28 SE-754 50 Uppsala, http://www.tdbcons.se.

35 T. Trongsatitkul and B. M. Budhlall, 2012, in review.

36 W.-F. Lee and W.-J. Lin, *J. Polym. Res.*, 2002, **9**, 23–29.

37 P. J. Flory. *Principles of Polymer Chemistry*; Cornell University Press, 1953.

38 S. Lu and K. S. Anseth, *Macromolecules*, 2000, **33**, 2509–2515.

39 E. W. Merrill, K. A. Dennison and C. Sung, *Biomaterials*, 1993, **14**, 1117–1126.

40 N. A. Peppas, P. Bures, W. Leobandung and H. Ichikawa, *Eur. J. Pharm. Biopharm.*, 2000, **50**, 19.

41 A. S. Hoffman, A. Afrassiabi and L. C. Dong, *J. Controlled Release*, 1986, **4**, 213–222.

42 Y. H. Bae, T. Okano, R. Hsu and S. W. Kim, *Makromol. Chem. Rapid Comm.*, 1987, **8**, 481–485.

43 S. W. Kim, Y. H. Bae and T. Okano, *Pharm. Res.*, 1992, **9**, 283–290.

44 H. M. Crowther and B. Vincent, *Colloid Polym. Sci.*, 1998, **276**, 46–51.

45 E. Daly and B. R. Saunders, *Phys. Chem. Chem. Phys.*, 2000, **2**, 3187–3193.

46 A. Guillermo, J. P. Cohen Addad, J. P. Bazile, D. Duracher, A. Elaissari and C. Pichot, *J. Polym. Sci., Part B: Polym. Phys.*, 2000, **38**, 889–898.

47 W. McPhee, K. C. Tam and R. H. Pelton, *J. Colloid Interface Sci.*, 1993, 156.

48 C. Alava and B. R. Saunders, *Colloids Surf., A*, 2005, **270–271**, 18–25.

49 R. W. Korsmeyer, R. Gurnya, E. Doelkera, P. Buria and N. A. Peppas, *Int. J. Pharm.*, 1983, **15**, 10.

50 A. Fick, *Ann. Phys.*, 1855, **94**, 59–86.

51 J. Crank, *The Mathematics of Diffusion*, Clarendon Press, Oxford, 1975.

52 C. S. Brazel and N. A. Peppas, *Macromolecules*, 1995, **28**, 8016–8020.

53 C. M. Hansen, Solubility Parameters, in *Hansen Solubility Parameters: A User's Handbook*, ed. C. M. Hansen, CRC Press, Taylor & Francis, Boca Raton, FL, 2nd edn, 2007.

54 R. Langer and N. Peppas, *J. Macromol. Sci., Part C: Polym. Rev.*, 1983, **23**, 61–126.

55 C. T. Reinhart and N. A. Peppas, *J. Membr. Sci.*, 1984, **18**, 227–239.